COMPUTATIONAL MECHANICS
New Trends and Applications
S. Idelsohn, E. Oñate and E. Dvorkin (Eds.)

FREE VIBRATIONS OF NONCIRCULAR ARCHES CONSIDERING ROTATORY INERTIA AND SHEAR DEFORMATION

Sang-Jin Oh[*], Byoung-Koo Lee[†], In-Won Lee[*], and Moon-Ho Park[††]

[*] Department of Civil Engineering
Korea Advanced Institute of Science and Technology
Taejon 305-701, Korea
e-mail: iwlee@cais.kaist.ac.kr

[†] Department of Civil and Environmental Engineering
Wonkwang University
Iksan, Junbuk 570-749, Korea
e-mail: bkleest@wonnms.wonkwang.ac.kr

[††] Department of Civil Engineering
Kyungpook National University
Taegu 702-701, Korea
e-mail: parkmh@kyungpook.ac.kr

Key words: Noncircular Arch, Free Vibration, Natural Frequency, Rotatory Inertia, Shear Deformation.

Abstract. *The differential equations governing free, in-plane vibrations of noncircular arches with uniform stiffness and constant mass per unit length, including the effects of rotatory inertia, shear deformation and axial deformation, are derived and solved numerically to obtain frequencies and mode shapes. The lowest four natural frequencies are calculated for parabolic, elliptic and sinusoidal geometries with hinged-hinged, hinged-clamped, and clamped-clamped end constraints. A wide range of arch rise to span length ratios, slenderness ratios, and two different values of shear parameter are considered. The agreement with results determined by means of a finite element method is good from an engineering viewpoint.*

1 INTRODUCTION

The problem of the free vibration of arches has become a subject of interest for many investigators due to its importance in many practical applications. The governing equations and the significant historical literature on the in-plane vibrations of elastic arches reported in references and their citations. Den Hartog[1], Wolf[2], Veletsos *et al.*[3], Laura *et al.*[4], Maurizi *et al.*[5] and Chidamparam and Leissa[6] calculated the natural frequencies of circular arches for various boundary conditions. For noncircular arches, Volterra and Morell[7], Romanelli and Laura[8], Wang[9], Gutierrez *et al.*[10], Lee and Wilson[11] and Oh[12] analyzed the free vibration of arches with various geometries. Although there is considerable research on the free vibration analysis of arches, most work has been done within the scope of Bernoulli-Euler or Rayleigh beam theory. These theories are recognized as adequate for the usual engineering problems. However, for arches having large cross-sectional dimensions in comparison with their span length, and for arches in which higher modes are required, the Timoshenko beam theory which considers the effects of rotatory inertia and shear deformation gives a better approximation to the true behavior.

Considerable research has been devoted to study the effects of rotatory inertia and shear deformation on straight beam vibrations. In the case of arches, Austin and Veletsos[13], Davis *et al.*[14], Irie *et al.*[15], Issa *et al.*[16], Kang *et al.*[17] and Yildirim[18] analyzed the free vibrations by the Timoshenko beam theory, but these are for only the simplest geometry, the circular arch.

The main purpose of this paper is to investigate the free vibrations of noncircular arches based on the Timoshenko beam theory. The differential equations are derived for the in-plane free vibration of linearly elastic arches of uniform stiffness and constant mass per unit length. The effects of rotatory inertia, shear deformation and axial deformation are included.

The governing equations were solved numerically for the parabolic, elliptic and sinusoidal geometries with hinged-hinged, hinged-clamped, and clamped-clamped end constraints. The effects of the arch rise to span length ratio, the slenderness ratio and the shear parameter on frequencies are investigated. The effects of rotatory inertia and shear deformation on frequencies of parabolic arches are reported.

2 MATHEMATICAL MODEL

The geometry of the noncircular arch with uniform cross-section, symmetric about the crown, is depicted in Figure 1(a). Its span length, rise, and shape of the middle surface are l, h, and $y(x)$, respectively. Its radius of curvature ρ, a function of the co-ordinate x, has an inclination ϕ with the x-axis. Shown in Figure 1(a) are the positive directions of radial and tangential displacements, w and v, and positive direction of the rotation angle ψ of the cross section at point ϕ.

A small element of the arch shown in Figure 1(b) defines the positive directions for its loads: the axial forces N; the shear forces Q; the bending moments M; the radial inertia force P_r; the tangential inertia force P_t; and rotatory inertia couple T. With the inertia forces and the inertia couple treated as equivalent static quantities, the three equations for "dynamic equilibrium" of the element are

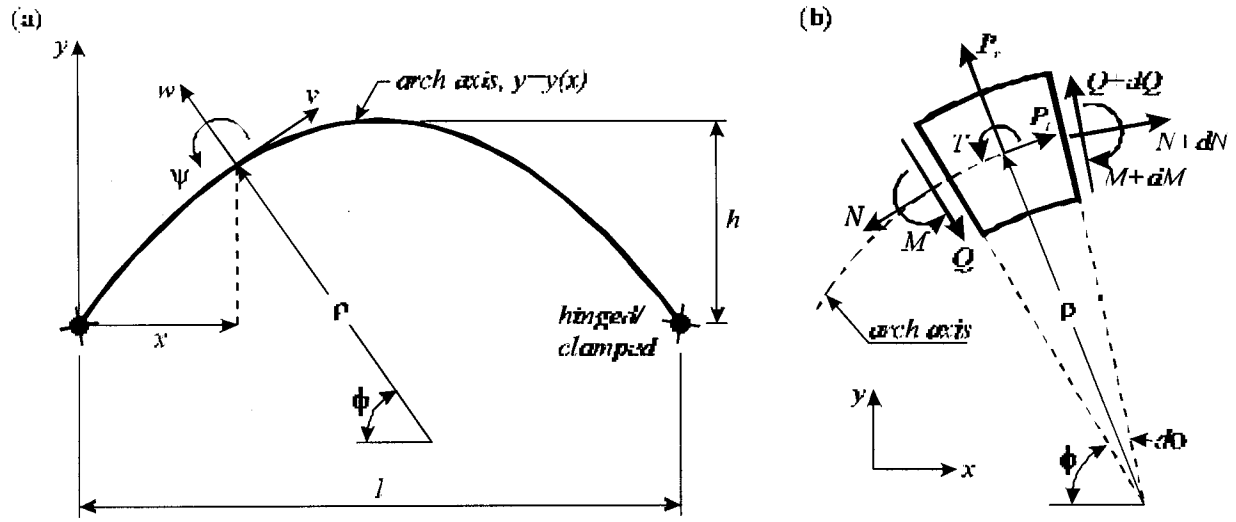

Figure 1. (a) Arch geometry; (b) loads on an arch element.

$$\frac{dN}{d\phi}+Q+\rho P_t=0, \tag{1}$$

$$\frac{dQ}{d\phi}-N+\rho P_r=0, \tag{2}$$

$$\frac{1}{\rho}\frac{dM}{d\phi}-Q-T=0. \tag{3}$$

The rotation of the tangent to the centroidal axis is given by equation (4), which is well-known[19],

$$\Phi=\frac{1}{\rho}\left(\frac{dw}{d\phi}-v\right). \tag{4}$$

When shear deformation is considered, normal plane cross sections do not remain plane and normal to the centroidal axis during deformation. However, an average rotation of the cross section can be found in the usual manner. The average rotation of the cross section will differ from the rotation of the tangent to the centroidal axis by the angular deformation β due to shear. Then, the rotation of the tangent to the centroidal axis may be expressed as

$$\Phi=\psi+\beta. \tag{5}$$

From equations (4) and (5) one obtains

$$\beta=\frac{1}{\rho}\left(\frac{dw}{d\phi}-v-\rho\psi\right). \tag{6}$$

From the elementary theory of beams, the bending moment, normal force and shear force are given, respectively, as[20]

$$M = -\frac{EI}{\rho}\psi', \tag{7}$$

$$N = \frac{EA}{\rho}(v' + w) + \frac{EI}{\rho^2}\psi', \tag{8}$$

$$Q = kAG\beta = \frac{kAG}{\rho}(w' - v - \rho\psi), \tag{9}$$

where $(')=d/d\phi$, E is the Young's modulus, I is the area moment of inertia of cross-section, A is the cross-sectional area, k is the shape factor of cross-section, and G is the shear modulus.

The arch is assumed to be in harmonic motion, or each co-ordinate is proportional to $\sin(\omega t)$, where ω is the angular frequency and t is time. The inertia loadings are then

$$P_r = \gamma A\omega^2 w, \tag{10}$$

$$P_t = \gamma A\omega^2 v, \tag{11}$$

$$T = \gamma I\omega^2 \psi, \tag{12}$$

where γ is mass density of arch material.

When equations (7), (8) and (9) are differentiated once, the results are

$$M' = -\frac{EI}{\rho}\psi'' + \frac{EI}{\rho^2}\rho'\psi', \tag{13}$$

$$N' = \frac{EA}{\rho}(v'' + w') - \frac{EA}{\rho^2}\rho'(v' + w) + \frac{EI}{\rho^2}\psi'' - \frac{2EI}{\rho^3}\rho'\psi', \tag{14}$$

$$Q' = \frac{kAG}{\rho}(w'' - v' - \rho'\psi - \rho\psi') - \frac{kAG}{\rho^2}\rho'(w' - v - \rho\psi). \tag{15}$$

To facilitate the numerical studies, the following non-dimensional system variables are defined. The arch rise to span length ratio f, the slenderness ratio s and the shear parameter μ are, respectively,

$$f = h/l, \quad s = l/\sqrt{I/A}, \quad \mu = kG/E. \tag{16-18}$$

The co-ordinates, the displacements and the radius of curvature are normalized by the span length l:

$$\xi = x/l, \ \eta = y/l; \quad \delta = w/l, \ \lambda = v/l; \quad \zeta = \rho/l. \tag{19-21}$$

The last is the frequency parameter,

$$C_i = \omega_i sl\sqrt{\gamma/E}, \tag{22}$$

which is written in terms of the ith frequency $\omega=\omega_i$, i=1,2,3,4,....

When equations (8), (10) and (15) are substituted into equation (2) and the non-dimensional forms of equations (16)-(22) are used, the result is

$$\delta'' = \zeta^{-1}\zeta'\delta' + \mu^{-1}(1-\zeta^2 s^{-2}C_i^2)\delta + (1+\mu^{-1})\lambda' - \zeta^{-1}\zeta'\lambda + (\zeta + \mu^{-1}\zeta^{-1}s^{-2})\psi'. \quad (23)$$

When equations (9), (11) and (14) are substituted into equation (1) and equations (16)-(22) are used, the result is

$$\lambda'' = \zeta^{-1}\zeta'\lambda' + (\mu - \zeta^2 s^{-2}C_i^2)\lambda - (1+\mu)\delta' + \zeta^{-1}\zeta'\delta - \zeta^{-1}s^{-2}\psi'' + 2\zeta^{-2}\zeta' s^{-2}\psi' + \mu\zeta\psi. \quad (24)$$

When equations (9), (12) and (13) are substituted into equation (3) and equations (16)-(22) are used, the result is

$$\psi'' = \zeta^{-1}\zeta'\psi' + (\mu s^2 - s^{-2}C_i^2)\zeta^2\psi - \zeta\mu s^2\delta' + \zeta\mu s^2\lambda. \quad (25)$$

The boundary conditions for hinged ends are

$$\delta = 0, \quad \lambda = 0, \quad \psi' = 0, \quad (26)$$

where the last condition assures that the moment M given by equation (7) is zero.

The boundary conditions for clamped ends are

$$\delta = 0, \quad \lambda = 0, \quad \psi = 0. \quad (27)$$

3 GEOMETRIC FUNCTIONS: ϕ, ζ AND ζ'

The geometric functions ϕ, ζ and ζ' contained in the governing differential equations (23)-(25) are computed as follows. The non-dimensional form of the given arch shape $y = y(x)$ is

$$\eta = \eta(\xi). \quad (28)$$

By definition

$$\phi = \frac{\pi}{2} - \tan^{-1}\left(\frac{d\eta}{d\xi}\right), \quad (29)$$

$$\zeta = \left(\frac{d^2\eta}{d\xi^2}\right)^{-1}\left[1 + \left(\frac{d\eta}{d\xi}\right)^2\right]^{3/2}. \quad (30)$$

Both ϕ and ζ are computed from derivatives of equation (28) and are expressed as functions of the single variable ξ. Then ζ' is calculated from the derivatives of equations (29) and (30) by using

$$\frac{d\zeta}{d\phi} = \frac{d\zeta}{d\xi}\frac{d\xi}{d\phi}. \quad (31)$$

The general equation for the parabolic arch of span length l and rise h is

$$y = -\frac{4h}{l^2}x(x-l), \quad 0 \le x \le l. \quad (32)$$

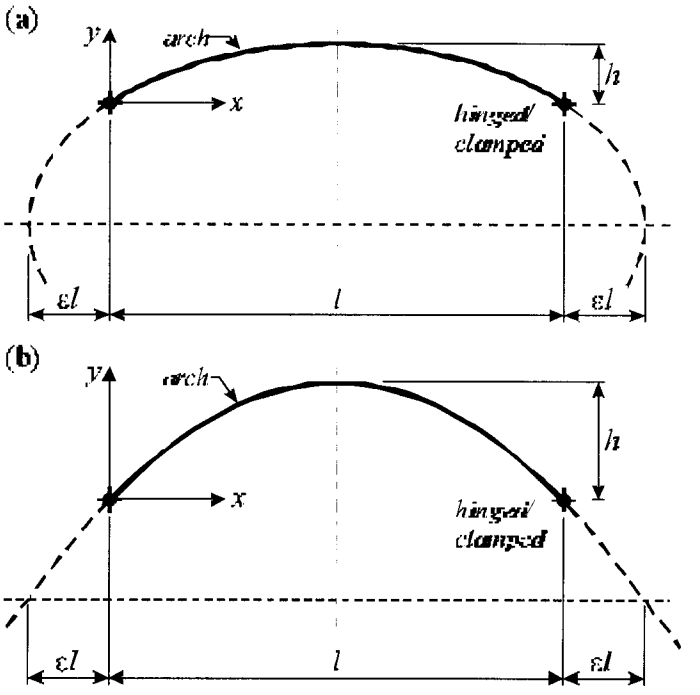

Figure 2. Arch shape: (a) elliptic; (b) sinusoidal.

With the equations (16) and (19), the non-dimensional form of equation (32) becomes

$$\eta = -4f\xi(\xi - 1), \quad 0 \le \xi \le 1. \tag{33}$$

With equation (33), the following geometric functions are calculated from equations (29)-(31):

$$\phi = \frac{\pi}{2} - \tan^{-1}[-4f(2\xi - 1)], \tag{34}$$

$$\zeta = \frac{1}{8f}[1 + 16f^2(2\xi - 1)^2]^{3/2}, \tag{35}$$

$$\zeta' = \frac{3}{2}(2\xi - 1)[1 + 16f^2(2\xi - 1)^2]^{3/2}. \tag{36}$$

Consider now an elliptic arch shown in Figure 2(a). This arch has span length l, rise h, and a co-ordinate system (x, y) originating from the left support. The corresponding ellipse curve, also shown in Figure 2(a), is composed of this arch segment and the broken line segments extending from each end. This ellipse curve of semimajor axis $L/2$ and semiminor axis H is expressed in terms of the (X, Y) co-ordinate system as

$$\frac{(X + L/2)^2}{(L/2)^2} + \frac{Y^2}{H^2} = 1. \tag{37}$$

The relationships between the two co-ordinate systems of Figure 2(a) are

(4) From the Runge-Kutta solution, evaluate at ξ=1 the determinant D of the coefficient matrix for the chosen set of three homogeneous boundary conditions. If D=0, then the trial value of C_i is an eigenvalue. If $D \neq 0$, then increment C_i and repeat the above calculations.
(5) Repeat Steps 3 and 4 and note the sign of D in each iteration. If D changes sign between two consecutive trials, then the eigenvalue lies between these last two trial values of C_i.
(6) Use the Regula-Falsi method to compute the advanced trial C_i based on its two previous values.
(7) Terminate the calculations and print the value of C_i and the corresponding mode shapes when the convergence criteria are met.

For these studies, suitable convergence of solutions was obtained for an increment of $\Delta\xi$=1/100. The convergence criterion was that C_i solutions obtained with a more crude increment of 1/30 agreed with those obtained with the 1/100 increment to within four significant figures.

5 NUMERICAL RESULTS

The first series of numerical studies are shown in Table 1. These studies served as an approximate check on the analysis presented herein. For comparison purpose, finite element solutions based on the package ADINA were used to compute the lowest four frequency parameters C_i for three cases: a hinged-hinged parabolic arch with f=0.3, s=75, and μ=0.3; a hinged-clamped elliptic arch with f=0.2, s=50, μ=0.3, and ε=0.5; and a clamped-clamped sinusoidal arch with f=0.1, s=100, μ=0.3, and ε=0.5. The agreement is good for all cases considered.

All of the numerical results that follow are based on the analysis reported herein. The results shown in Figures 3~5, depict the variation of frequency parameters C_i of parabolic arches with f. A value of μ=0.1 corresponds to a wide-flange steel section, and μ=0.3 corresponds

Table 1. Comparison of results between finite element solutions (ADINA) and this study.

Geometry of arch	i	Frequency parameter, C_i	
		ADINA	This study
Parabolic	1	21.81	21.83
hinged-hinged,	2	55.80	56.00
f=0.3, s=75,	3	101.7	102.3
μ=0.3	4	113.4	113.4
Elliptic(ε=0.5)	1	35.26	35.25
hinged-clamped,	2	56.99	57.11
f=0.2, s=50,	3	83.05	83.00
μ=0.3	4	128.1	128.2
Sinusoidal(ε=0.5)	1	56.25	56.30
clamped-clamped,	2	66.25	66.14
f=0.1, s=100,	3	114.9	114.3
μ=0.3	4	181.7	181.7

approximately to a solid rectangular metal section. Additional data, obtained by a theory which neglects the effects of rotatory inertia and shear deformation, are available in reference [12]. In these figures, several of the frequency parameters reach a peak as the rise to span length ratio f is increased. The effects of rotatory inertia and shear deformation become more important as the shear parameter μ is small. Where the curves met (Figures 3 and 5), two mode shapes may exist at a single frequency.

Figures 6~8 show the variation of frequency parameters C_i with s. The figures show that the curves are a combination of plateaus and diagonal lines. The curves demonstrate that the effects of rotatory inertia and shear deformation tend to smooth the curves and are more prominent around the convex corners. The effects become more important where the slenderness ratio and the shear parameter are small.

Shown in Figure 9 are the computed frequency parameters C_i and their corresponding mode shapes for hinged-hinged, hinged-clamped and clamped-clamped parabolic arches with f=0.2, s=50, and μ=0.1.

Tables 2~4 depict the lowest four values of the frequency parameters C_i for parabolic, elliptic and sinusoidal geometries with hinged-hinged, hinged-clamped and clamped-clamped end constraints. These results show that, for a given set of arch parameters and matching end constraints, the arch geometry has little effect on the frequency parameters C_i.

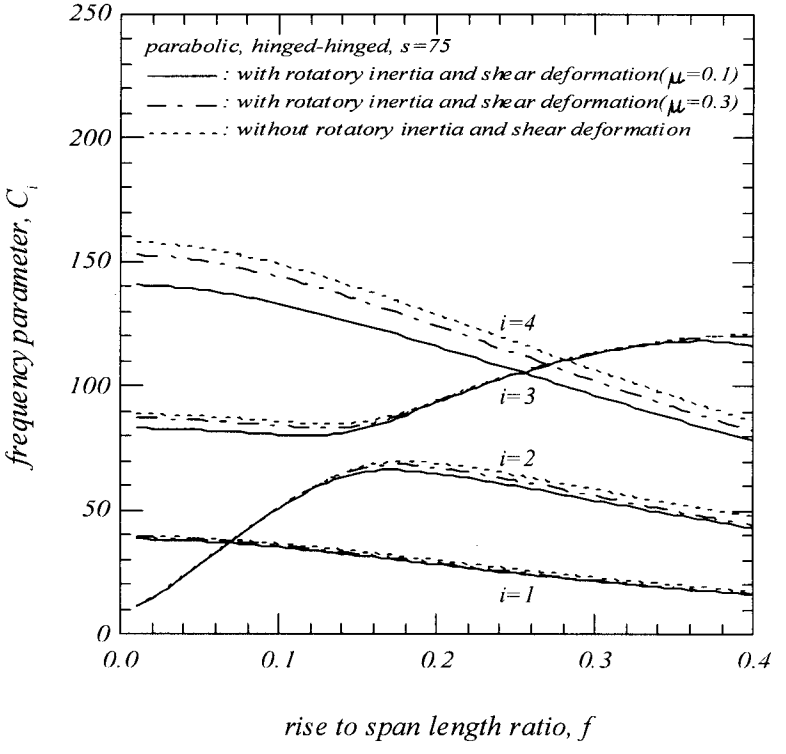

Figure 3. Effect of f on frequency parameter C_i for hinged-hinged parabolic arches.

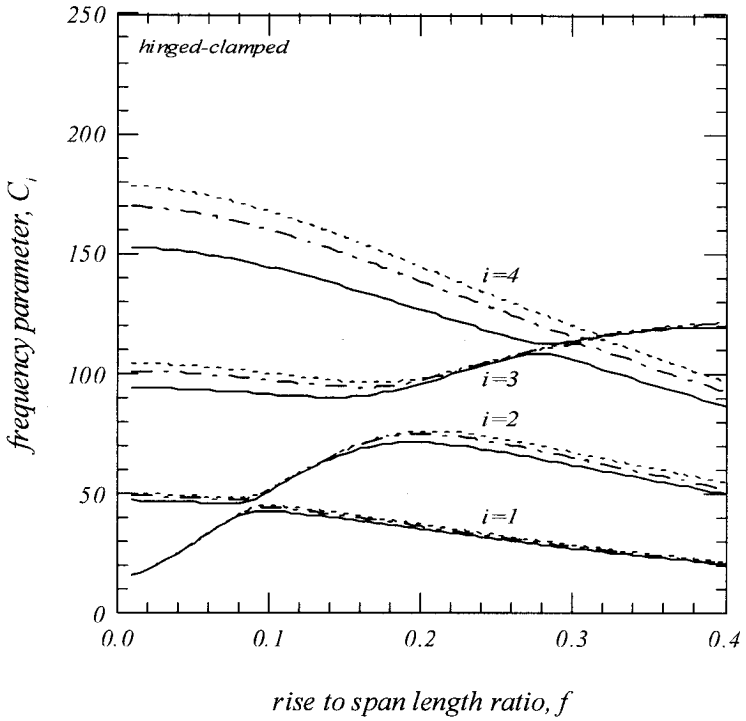

Figure 4. Effect of f on frequency parameter C_i for hinged-clamped parabolic arches.

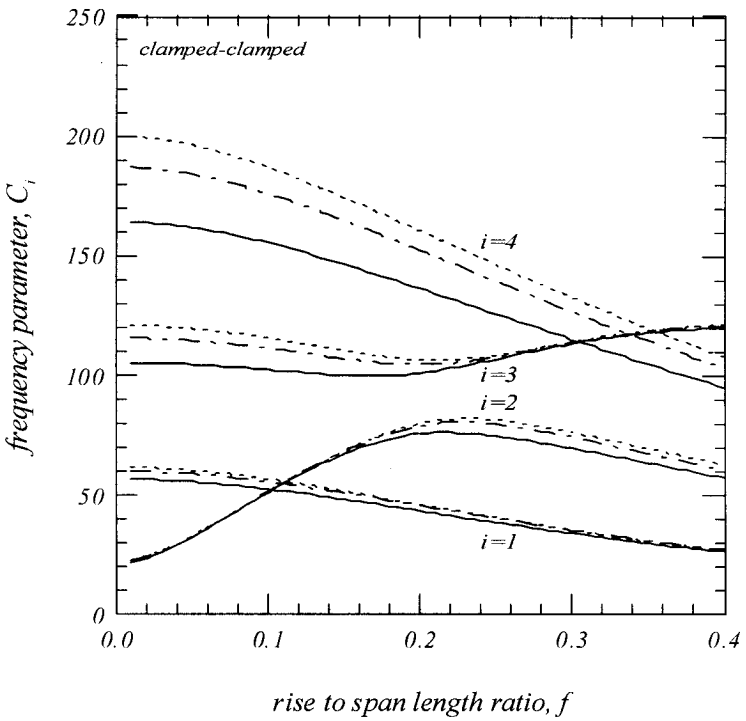

Figure 5. Effect of f on frequency parameter C_i for clamped-clamped parabolic arches.

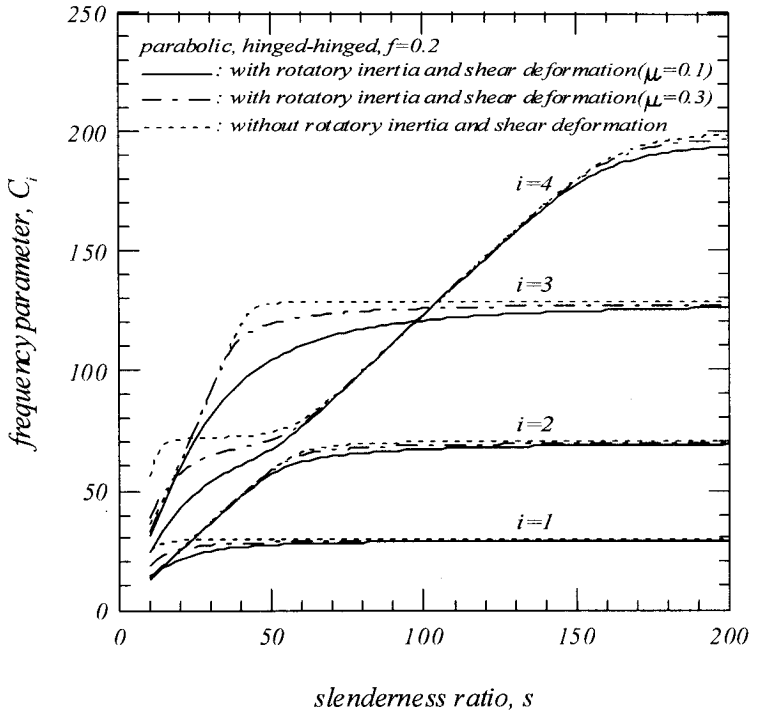

Figure 6. Effect of s on frequency parameter C_i for hinged-hinged parabolic arches.

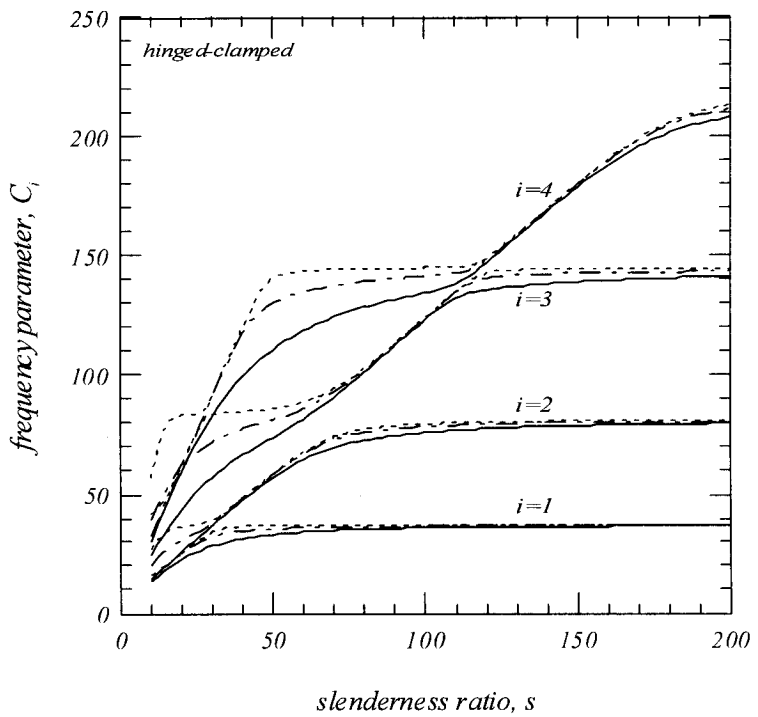

Figure 7. Effect of s on frequency parameter C_i for hinged-clamped parabolic arches.

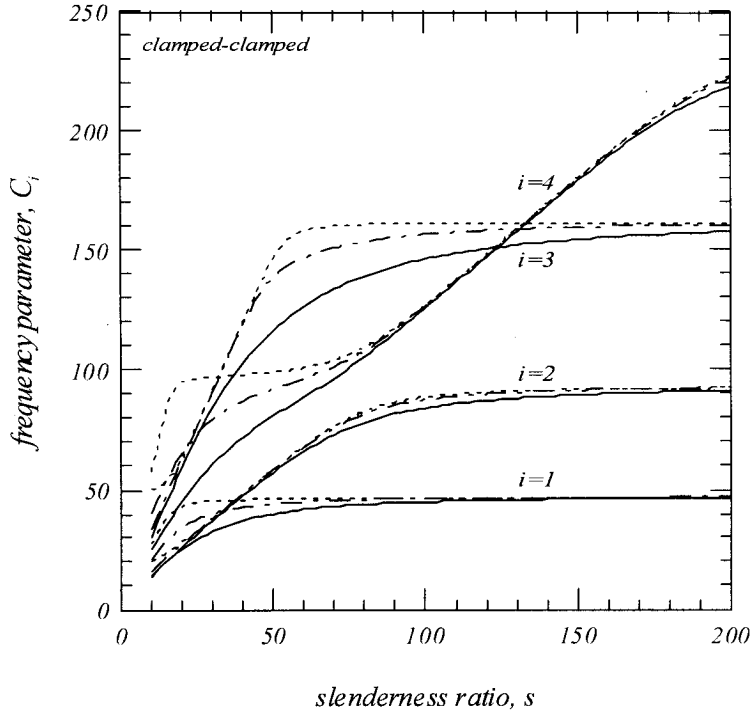

Figure 8. Effect of s on frequency parameter C_i for clamped-clamped parabolic arches.

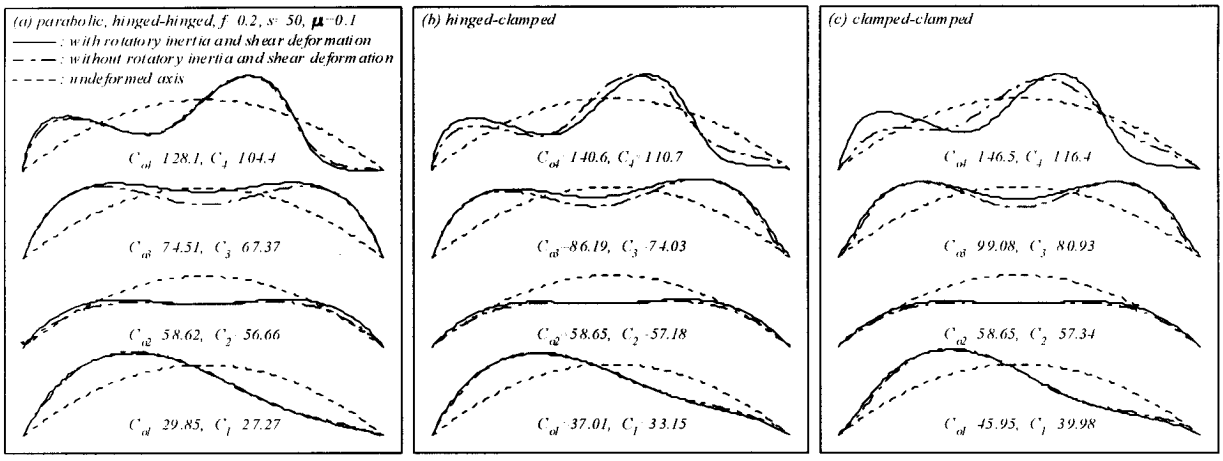

Figure 9. Examples of mode shapes.

6 CONCLUSIONS

The governing differential equations for noncircular arches, including the effects of rotatory inertia, shear deformation and axial deformation, are derived and solved numerically. There is a very good agreement between the results of the present analysis and ADINA. For the parabolic arches, the effects of rotatory inertia and shear deformation on C_i were analyzed. For three

Table 2. Frequency parameter C_i of hinged-hinged arches.

F	s	Shape	μ=0.1				μ=0.3			
			Frequency parameter, C_i				Frequency parameter, C_i			
			i=1	i=2	i=3	i=4	i=1	i=2	i=3	i=4
0.01	30	Parabolic	9.650	33.23	63.77	94.16	9.974	37.47	79.21	94.25
		Elliptic	9.654	33.23	63.77	94.10	9.979	37.46	79.21	94.25
		Sinusoidal	9.646	33.24	63.77	94.19	9.971	37.47	79.21	94.25
	60	Parabolic	10.66	37.61	80.15	133.0	10.74	38.94	86.25	149.9
		Elliptic	10.68	37.61	80.16	133.0	10.76	38.94	86.26	149.9
		Sinusoidal	10.65	37.61	80.15	133.0	10.73	38.94	86.25	149.9
	100	Parabolic	12.17	38.76	85.43	147.5	12.20	39.26	87.88	154.9
		Elliptic	12.22	38.76	85.45	147.5	12.25	39.26	87.91	154.9
		Sinusoidal	12.15	38.76	85.41	147.5	12.17	39.26	87.87	154.9
0.1	30	Parabolic	22.31	30.54	60.93	89.71	22.48	34.21	74.94	93.87
		Elliptic	22.39	30.40	61.08	88.57	22.59	34.05	75.00	93.82
		Sinusoidal	22.23	30.64	60.86	90.52	22.38	34.32	74.93	93.84
	60	Parabolic	34.48	41.53	76.92	126.0	35.64	41.67	82.26	141.1
		Elliptic	34.33	41.32	77.80	125.3	35.47	41.56	83.02	140.2
		Sinusoidal	34.59	41.57	76.44	126.4	35.75	41.66	81.86	141.6
	100	Parabolic	35.51	64.24	86.66	139.4	35.95	64.76	88.35	146.0
		Elliptic	35.35	62.03	90.24	138.8	35.79	62.69	91.79	145.3
		Sinusoidal	35.62	65.72	84.31	139.7	36.06	66.10	86.14	146.4
0.2	30	Parabolic	24.80	36.50	53.72	81.56	27.40	36.79	64.52	91.23
		Elliptic	24.49	36.21	54.29	80.29	27.04	36.75	64.73	91.01
		Sinusoidal	25.03	36.59	53.48	82.36	27.66	36.74	64.48	91.18
	60	Parabolic	27.76	61.71	76.63	110.4	28.57	64.64	77.88	122.2
		Elliptic	27.40	59.26	79.90	109.3	28.20	61.99	81.33	120.8
		Sinusoidal	28.02	63.45	74.40	111.0	28.84	66.64	75.41	122.9
	100	Parabolic	28.52	67.10	120.8	123.1	28.83	68.68	123.3	125.9
		Elliptic	28.15	65.24	119.8	126.4	28.46	66.74	124.7	126.8
		Sinusoidal	28.79	68.18	121.2	121.5	29.10	69.80	121.3	126.6
0.4	30	Parabolic	14.78	36.11	49.20	60.04	15.86	41.58	49.28	73.95
		Elliptic	14.44	35.85	49.46	59.73	15.48	41.22	49.58	73.85
		Sinusoidal	15.04	36.14	49.21	60.13	16.14	41.56	49.38	73.46
	60	Parabolic	16.11	42.10	75.66	97.29	16.42	43.96	81.37	97.77
		Elliptic	15.72	41.79	75.15	97.62	16.03	43.61	80.79	98.19
		Sinusoidal	16.40	42.21	75.94	97.23	16.71	44.08	81.69	97.68
	100	Parabolic	16.43	43.77	80.71	124.8	16.52	44.49	83.02	130.1
		Elliptic	16.04	43.44	80.13	123.9	16.13	44.14	82.41	129.2
		Sinusoidal	16.72	43.91	81.05	125.3	16.81	44.63	83.38	130.7

Table 3. Frequency parameter C_i of hinged-clamped arches.

f	s	Shape	μ=0.1				μ=0.3			
			Frequency parameter, C_i				Frequency parameter, C_i			
			i=1	i=2	i=3	i=4	i=1	i=2	i=3	i=4
0.01	30	Parabolic	13.71	37.67	66.99	94.20	14.91	45.11	87.30	94.25
		Elliptic	13.71	37.67	66.99	94.16	14.91	45.11	87.30	94.25
		Sinusoidal	13.71	37.67	66.99	94.22	14.91	45.11	87.30	94.25
	60	Parabolic	15.44	45.81	89.55	142.1	15.79	48.61	99.29	165.2
		Elliptic	15.45	45.81	89.56	142.0	15.80	48.61	99.29	165.1
		Sinusoidal	15.44	45.81	89.54	142.1	15.79	48.62	99.28	165.2
	100	Parabolic	16.70	48.33	98.20	162.3	16.82	49.45	102.4	173.3
		Elliptic	16.71	48.33	98.20	162.3	16.83	49.44	102.4	173.2
		Sinusoidal	16.69	48.33	98.19	162.3	16.81	49.45	102.4	173.3
0.1	30	Parabolic	23.53	35.05	64.30	90.59	24.08	41.61	82.93	93.88
		Elliptic	23.53	34.90	64.47	89.46	24.10	41.44	83.00	93.82
		Sinusoidal	23.51	35.16	64.21	91.39	24.06	41.75	82.89	93.88
	60	Parabolic	39.62	44.22	86.26	134.6	40.48	46.00	94.87	155.1
		Elliptic	39.75	43.60	86.98	133.8	40.60	45.46	95.43	153.9
		Sinusoidal	39.48	44.66	85.83	135.1	40.34	46.40	94.54	155.8
	100	Parabolic	44.12	64.54	97.86	153.6	45.09	65.00	101.1	163.4
		Elliptic	44.15	62.70	100.3	152.9	45.13	63.31	103.4	162.6
		Sinusoidal	44.08	65.79	96.28	154.0	45.04	66.14	99.70	163.8
0.2	30	Parabolic	28.33	37.10	57.42	83.17	32.37	38.31	72.17	91.23
		Elliptic	28.11	36.59	58.00	81.74	32.25	37.87	72.39	91.05
		Sinusoidal	28.49	37.39	57.11	84.14	32.44	38.61	72.07	91.22
	60	Parabolic	34.23	64.76	81.63	118.6	35.97	67.20	85.93	134.8
		Elliptic	33.98	62.13	84.54	117.4	35.73	64.82	88.51	133.2
		Sinusoidal	34.40	66.75	79.50	119.4	36.14	68.91	84.15	135.8
	100	Parabolic	35.98	75.98	122.9	134.2	36.68	78.54	123.5	141.5
		Elliptic	35.72	73.44	125.3	133.7	36.42	75.87	126.5	140.4
		Sinusoidal	36.16	77.62	121.2	134.7	36.86	80.29	121.6	142.1
0.4	30	Parabolic	17.77	39.41	49.43	62.72	19.86	47.00	49.97	78.28
		Elliptic	17.47	38.85	49.86	62.33	19.52	45.73	51.02	78.11
		Sinusoidal	18.00	39.63	49.32	62.87	20.11	47.66	49.48	77.53
	60	Parabolic	20.39	48.53	82.81	97.31	21.09	51.63	91.07	97.77
		Elliptic	20.05	47.99	82.15	97.63	20.74	51.04	90.25	98.22
		Sinusoidal	20.65	48.79	83.19	97.28	21.36	51.93	91.53	97.68
	100	Parabolic	21.11	51.41	90.26	134.6	21.36	52.66	93.77	141.6
		Elliptic	20.75	50.86	89.53	133.6	21.01	52.09	93.00	140.4
		Sinusoidal	21.37	51.69	90.69	135.3	21.62	52.95	94.24	142.3

Table 4. Frequency parameter C_i of clamped-clamped arches.

f	s	Shape	μ=0.1				μ=0.3			
			Frequency parameter, C_i				Frequency parameter, C_i			
			i=1	i=2	i=3	i=4	i=1	i=2	i=3	i=4
0.01	30	Parabolic	18.10	41.68	69.96	94.21	20.75	52.72	94.25	95.00
		Elliptic	18.10	41.68	69.96	94.19	20.75	52.72	94.25	95.00
		Sinusoidal	18.10	41.68	69.96	94.22	20.75	52.72	94.25	95.00
	60	Parabolic	21.37	54.18	98.70	150.7	22.26	59.05	112.7	180.4
		Elliptic	21.37	54.18	98.70	150.7	22.25	59.04	112.7	180.3
		Sinusoidal	21.38	54.18	98.69	150.7	22.27	59.05	112.7	180.4
	100	Parabolic	22.83	58.62	111.3	177.2	23.17	60.66	117.8	192.3
		Elliptic	22.81	58.62	111.4	177.2	23.15	60.66	117.8	192.3
		Sinusoidal	22.85	58.63	111.3	177.2	23.18	60.67	117.8	192.3
0.1	30	Parabolic	25.93	38.85	67.42	91.14	27.43	48.71	90.62	93.88
		Elliptic	25.80	38.73	67.60	90.06	27.29	48.57	90.67	93.82
		Sinusoidal	26.01	38.94	67.31	91.88	27.52	48.82	90.60	93.88
	60	Parabolic	42.89	50.36	95.36	142.7	43.26	54.69	107.9	168.0
		Elliptic	42.28	50.23	95.98	141.7	42.71	54.56	108.3	166.3
		Sinusoidal	43.29	50.45	94.97	143.3	43.63	54.79	107.6	169.2
	100	Parabolic	54.39	64.61	110.1	167.6	56.21	65.04	115.4	181.2
		Elliptic	54.26	62.85	111.9	166.8	56.08	63.43	117.0	180.4
		Sinusoidal	54.49	65.81	108.9	168.1	56.30	66.14	114.3	181.7
0.2	30	Parabolic	32.71	37.27	60.83	84.41	38.11	40.17	79.68	91.23
		Elliptic	32.42	36.69	61.41	82.87	37.71	39.85	79.87	91.06
		Sinusoidal	32.91	37.62	60.50	85.51	38.37	40.42	79.60	91.23
	60	Parabolic	41.78	66.01	88.59	126.2	44.96	67.95	96.53	146.9
		Elliptic	41.45	63.52	91.03	124.7	44.62	65.89	98.40	144.8
		Sinusoidal	42.01	67.82	86.86	127.2	45.21	69.37	95.30	148.3
	100	Parabolic	44.84	84.10	125.6	146.2	46.16	87.63	126.5	156.7
		Elliptic	44.51	80.76	128.8	144.8	45.82	84.07	129.9	155.1
		Sinusoidal	45.09	86.45	123.4	147.1	46.41	90.17	124.2	157.7
0.4	30	Parabolic	21.18	42.26	49.92	65.15	24.72	48.63	54.58	78.35
		Elliptic	20.85	41.33	50.66	64.63	24.34	47.49	55.40	78.38
		Sinusoidal	21.42	42.76	49.59	65.37	25.00	49.30	54.17	78.03
	60	Parabolic	25.63	55.05	89.87	97.32	26.96	59.78	97.77	101.1
		Elliptic	25.23	54.26	89.13	97.63	26.54	58.87	98.22	100.2
		Sinusoidal	25.92	55.47	90.30	97.29	27.27	60.27	97.68	101.6
	100	Parabolic	26.97	59.52	100.1	143.4	27.48	61.51	105.1	150.9
		Elliptic	26.55	58.75	99.21	142.1	27.06	60.71	104.1	149.7
		Sinusoidal	27.28	59.94	100.6	144.2	27.79	61.96	105.6	151.8

arch geometries(parabolic, elliptic and sinusoidal), the effects of each of the three parameters f, s and μ on C_i were investigated.

REFERENCES

[1] J.P. Den Hardog, "The lowest natural frequency of circular arcs", *Philosophical Magazine*, 5, 400-408 (1928).

[2] J.A. Wolf, Jr., "Natural frequencies of circular arches", *Journal of the Structural Division*, ASCE, 97, 2337-2350 (1971).

[3] A.S. Veletsos, W.J. Austin, C.A.L. Pereira and S.J. Wung, "Natural frequencies of circular arches", *Journal of the Engineering Mechanic Division*, ASCE, 98, 311-329 (1972).

[4] P.A.A. Laura, P.L. Verniere De Irassar, R. Carnicer and R. Bertero, "A note on vibrations of a circumferential arch with thickness varying in a discontinuous fashion", *Journal of Sound and Vibration*, 120, 95-105 (1988).

[5] M.J. Maurizi, R.E. Rossi and P.M. Belles, "Lowest natural frequency of clamped circular arcs of linearly tapered width", *Journal of Sound and Vibration*, 144, 357-361 (1991).

[6] P. Chidamparam and A.W. Leissa, "Influence of centerline extensibility on the in-plane free vibrations of loaded circular arches", *Journal of Sound and Vibration*, 183, 779-795 (1995).

[7] E. Volterra and J.D. Morell, "A note on the lowest natural frequency of elastic arcs", *Journal of Applied Mechanics*, ASME, 27, 744-746 (1960).

[8] E. Romanelli and P.A.A. Laura, "Fundamental frequencies of non-circular, elastic, hinged arcs", *Journal of Sound and Vibration*, 24, 17-22 (1972).

[9] T.M. Wang, "Effect of variable curvature on fundamental frequency of clamped parabolic arcs", *Journal of Sound and Vibration*, 41, 247-251 (1975).

[10] R.H. Gutierrez, P.A.A. Laura, R.E. Rossi, R. Bertero and A. Villaggi, "In-plane vibrations of non-circular arcs of non-uniform cross-section", *Journal of Sound and Vibration*, 129, 181-200 (1989).

[11] B.K. Lee and J.F. Wilson, "Free vibrations of arches with variable curvature", *Journal of Sound and Vibration*, 136, 75-89 (1989).

[12] S.J. Oh, "Free vibrations of arches with variable cross-section", Ph.D. Thesis, Wonkwang University, (1997).

[13] W.J. Austin and A.S. Veletsos, "Free vibration of arches flexible in shear", Journal of Engineering Mechanics Division, ASCE, 99, 735-753 (1973).

[14] R. Davis, R.D. Henshell and G.B. Warburton, "Constant curvature beam finite elements for in-plane vibration", *Journal of Sound and Vibration*, 25, 561-576 (1972).

[15] T. Irie, G. Yamada and K. Tanaka, "Natural frequencies of in-plane vibration of arcs", Journal of Applied Mechanic, ASME, 50, 449-452 (1983).

[16] M.S. Issa, T.M. Wang and B.T. Hsiao, "Extensional vibrations of continuous circular curved beams with rotary inertia and shear deformation, I: Free Vibration", *Journal of Sound and Vibration*, 114, 297-308 (1987).

[17] K. Kang, C.W. Bert and A.G. Striz, "Vibration analysis of shear deformable circular arches by the differential quadratic method", *Journal of Sound and Vibration*, 181, 353-360, (1995).
[18] V. Yildirim, "A computer program for the free vibration analysis of elastic arcs", Computers & Structures, 62, 475-485 (1997).
[19] J. Henrych, *The dynamics of arches and frames*, Elsevier Scientific Publishing Company, (1981).
[20] S.F. Borg and J.J. Gennaro, *Advanced structural analysis*, D. Van Nostrand Company, (1959).